Soft Matter

PAPER

View Article Online
View Journal | View Issue

Cite this: *Soft Matter*, 2022, **18**, 4786

The effects of surface hydration on capillary adhesion under nanoscale confinement†

Sijia Huang,[a] Carlos E. Colosqui,*[ab] Y.-N. Young[c] and Howard A. Stone[d]

Received 14th April 2022,
Accepted 2nd June 2022

DOI: 10.1039/d2sm00473a

rsc.li/soft-matter-journal

Nanoscale phenomena such as surface hydration and the molecular layering of liquids under strong nanoscale confinement play a critical role in liquid-mediated surface adhesion that is not accounted for by available models, which assume a uniform liquid density with or without considering surface forces and associated disjoining pressure effects. This work introduces an alternative theoretical description that *via* the potential of mean force (PMF) considers the strong spatial variation of the liquid number density under nanoscale confinement. This alternative description based on the PMF predicts a dual effect of surface hydration by producing: (i) strong spatial oscillations of the local liquid density and pressure and, more importantly, (ii) a configuration-dependent liquid–solid surface energy under nanoscale confinement. Theoretical analysis and molecular dynamics simulations for the case of an axisymmetric water bridge with nanoscale heights show that the latter hydration effect is critical for the accurate prediction of the surface energy and adhesion forces when a small volume of liquid is nanoscopically confined by two surfaces approaching contact.

Introduction

Nanoscale contact mediated by liquid wetting processes and the adhesion forces produced by nanoscale capillary bridges are relevant to numerous and diverse nanofabrication methods such as capillary-driven self-assembly of nanomaterials,[1–5] capillary force lithography,[6,7] capillary-assisted sintering and welding,[8,9] and additive manufacturing,[10–12] among many others. Furthermore, the accurate prediction of adhesion forces produced by nanoscale water bridges is critically important for the application and interpretation of nanoscale characterization methods based on atomic force microscopy.[13–17]

The conventional continuum thermodynamics approach to predict equilibrium configurations and the associated capillary forces in interfacial systems varying from macro- to nanoscale is to solve the Young–Laplace (Y–L) equation.[18–21] The conventional description based on the Y–L equation assumes perfectly homogeneous phases with uniform number density and pressure. Moreover, the equilibrium contact angle is commonly defined in terms of the surface energies by invoking some form of the Young's law. Augmented versions of the Y–L equation, while still considering a perfectly uniform liquid density, have included local variations of the disjoining/conjoining pressure that are predicted *via* Derjaguin–Landau–Verwey–Overbeek (DLVO) theory.[22–27] However, molecular liquids under nanoscale confinement in the sub-10 nm range present strong spatial variations of the liquid density that are associated with molecular layering and surface hydration forces.[28–30] In particular, hydration forces for crystalline or quasi-crystalline surfaces exhibit spatial oscillations with a period comparable to the water molecule diameter and decay over a few molecular layers away from the wall.[30–32]

In this work we adopt and extend the description based on the Y–L equation to consider local density variations in the liquid due to molecular layering and surface hydration, and apply the proposed alternative description to the particular case of liquid water bridges with nanoscale heights and a much larger (micro/macroscale) contact radius, which is a configuration commonly observed when a small volume of water is nanoscopically confined by two surfaces approaching contact. The key element of our alternative "augmented" description is incorporating in the Y–L equation the potential of mean force (PMF) that under thermodynamic equilibrium is obtained from the local liquid density profile, which can be determined by experimental and computational methods, or modeled by analytical expressions. By comparing predictions from the conventional description assuming a uniform liquid density and the proposed augmented description considering local

[a] *Applied Mathematics & Statistics Department, Stony Brook University, Stony Brook, NY 11794, USA*
[b] *Mechanical Engineering Department, Stony Brook University, Stony Brook, NY 11794, USA. E-mail: carlos.colosqui@stonybrook.edu*
[c] *Department of Mathematical Sciences, New Jersey Institute of Technology, Newark, NJ 07102, USA*
[d] *Department of Mechanical and Aerospace Engineering, Princeton University, Princeton, NJ 08544, USA*

† Electronic supplementary information (ESI) available. See DOI: https://doi.org/10.1039/d2sm00473a

density variations against results from molecular dynamics (MD) simulations, we aim to elucidate the critical dual effect of surface hydration on the local liquid pressure and liquid–solid surface energy and determine the relative importance of these effects.

Theoretical description

In the framework of sharp-interface continuum thermodynamics, the equilibrium shape of an axisymmetric capillary bridge (Fig. 1a) confined between two identical and perfectly plane walls is governed by the axisymmetric Y–L equation

$$\Delta p = \gamma\left[\frac{1}{r(1+\dot{r}^2)^{1/2}} - \frac{\ddot{r}}{(1+\dot{r}^2)^{3/2}}\right], \quad (1)$$

where $r = r(z)$ is the local bridge radius, $\dot{r} \equiv \mathrm{d}r/\mathrm{d}z$, $\ddot{r} \equiv \mathrm{d}^2r/\mathrm{d}z^2$, γ is the surface tension of the free surface, and $\Delta p = p - p_a$ is the difference between the liquid pressure, p, and ambient pressure, p_a. For the bridge heights considered here the gravitational effects are negligible. Finding a unique solution $r(z)$ of eqn (1) requires a proper set of boundary conditions corresponding to minimization of the system free energy, and satisfying the additional constraint $2\pi\int_0^{h/2} r^2\mathrm{d}z = V$ where V is the bridge volume.

We will consider the case of sufficiently large bridge volumes $V \gg \pi h\sigma^2$, where σ is the characteristic molecular diameter, so that the local bridge radius is $r(z) \gg \sigma$ and we can thus neglect radial variations of the liquid number density. Mechanical equilibrium for a perfectly homogeneous liquid phase with a sharp solid–liquid interface at $z = \pm z_w$ corresponds to $p(\bar{n}, T) = \bar{p} = \text{const.}$ and the equilibrium density profile $\bar{n}(z) = \{n_b \text{ for } |z| < z_w;\ 0 \text{ for } |z| = z_w\}$, where $n_b(T, p)$ is the bulk number density determined by an equation of state. For an inhomogeneous liquid in thermodynamic equilibrium with a local number density profile $n(z)$, we have the PMF $w = -k_BT\ln(n/\bar{n})$ (k_B is the Boltzmann constant) and hydrostatic equilibrium $\nabla p + n\nabla w = 0$ dictates that

$$\Delta p(z) = \Delta\bar{p} + k_BT\,(n - \bar{n}), \quad (2)$$

where $\Delta\bar{p} = \bar{p} - p_a$ is the pressure difference for the uniform liquid phase, assuming that $p_a = \text{const.}$ Additionally, we consider that for two identical parallel surfaces separated at a nanoscale height h, the solid–liquid surface energy is $\gamma_{SL}(h) = \gamma_S + \int_0^{h/2} nw\mathrm{d}z$, where γ_S is the solid surface energy (*i.e.*, the solid–vacuum interfacial surface energy). Further assuming constant liquid–vapor surface tension and a much less dense ambient phase, for which the solid–vapor surface energy is $\gamma_{SV} \simeq \gamma_S$, we invoke the conventional Young equation, $\cos\theta_Y = (\gamma_{SV} - \gamma_{SL})/\gamma$, to define the height-dependent Young contact angle

$$\cos\,\theta_Y(h) = \frac{k_BT}{\gamma}\int_0^{h/2} n\ln(n/n_b)\mathrm{d}z. \quad (3)$$

We note here that eqn (3) stresses that liquid molecular structure with spatial variation of the local number density over a finite length near the solid–liquid interface is necessary to observe non-neutral wetting conditions for which $\gamma_{SL} \neq \gamma_{SV}$ and $\theta_Y \neq 90$ deg.

For the studied nanoscale bridges, the height-dependent Young contact angle in eqn (3) will be employed to prescribe the equilibrium contact angle $\theta(h) = \pi/2 - \arctan[\dot{r}(z_w)] = \theta_Y$ by virtue of Young's law. It is worth noting that the variation of the Young contact angle predicted by eqn (3) is insensitive to the contact radius variation and thus is fundamentally different from a line tension effect. Considering the equilibrium contact angle $\theta = \theta_Y(h)$ as a function of only the bridge height h is a valid approximation for sufficiently large volumes $V \gg \pi h\sigma^2$ for which $r(z) \gg \sigma$. For such conditions line tension effects can be neglected since $\tau r_c \ll \gamma\cos\theta_Y r_c^2$, and the line tension/and surface tension $\gamma \sim \varepsilon/\sigma^2$ scale with the characteristic cohesive energy per molecule ε.

For the studied static conditions, the static adhesion force is

$$F(h) = -\Delta p_c\pi r_c^2 + 2\gamma\pi r_c\sin\theta_Y(h), \quad (4)$$

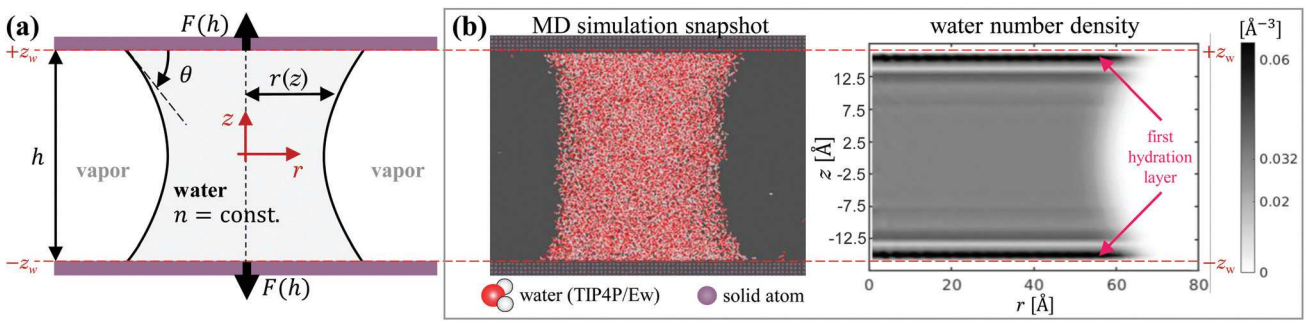

Fig. 1 Axisymmetric capillary bridge between two plane walls. (a) Conventional continuum description: all phases are perfectly uniform with a constant number density. A sharp liquid–vapor interface determines the local bridge radius $r(z)$ and the contact angle $\theta = \pi/2 - \arctan[\dot{r}(z_w)]$ where $z_w = h/2$. (b) Molecular dynamics: the water molecules (TIP4P/Ew model) form diffuse interfaces between the liquid, vapor, and solid phases. The top/bottom wall position $z = \pm z_w$ is defined at the position of contact between the water molecules and solid wall atoms. The local number density (averaged over the angular coordinate) shows significant spatial oscillations along the z-coordinate due to the formation of hydration layers, and a diffuse water–vapor interface with a thickness much smaller than the local bridge radius.

where $r_c = r(\pm h/2)$ and $\Delta p_c = \Delta p(\pm h/2)$ are determined *via* solution of eqn (1) and (2), and the equilibrium contact angle $\theta_Y(h)$ is given by eqn (3). We remark that eqn (4) can be used to determine the contact angle from the adhesion force, rather than from the radius slope $\dot{r}(z_w)$ at the wall.

Molecular dynamics

To verify the assumptions in the augmented Y–L model given by eqn (1)–(4), we perform fully atomistic non-equilibrium MD simulations of nanoscale capillary bridges of liquid water between two plane surfaces as shown in Fig. 1b. The MD simulations are performed in the *NVT* ensemble using the open-source code LAMMPS;[33] full technical details are described in the ESI.† [34] The MD simulations use conventional Lennard–Jones and Coulombic potentials[34] that model (i) hard core repulsion, van der Waals, and electrostatic interactions between the water molecules and (ii) hard core repulsion and van der Waals interactions between the solid material and water molecules. The solid is modeled as a "frozen" face-centered cubic lattice (fcc) of non-polar and neutrally charged atoms.

The water molecules are modeled by the TIP4P/Ew model,[35] which at the simulated system temperature $T = 300$ K reproduces the p–n–T phase diagram and structural properties of liquid water,[36, 37] with a slightly lower mass density $\rho = 964$ kg m^{-3} that corresponds to a bulk number density $n_b = 0.0322$ Å^{-3}, and surface tension $\gamma = 65.4$ mN m^{-1}.[38] The modeled water molecules have an effective diameter $\sigma = 0.355$ nm and the solid wall atoms are arranged in a fcc lattice with constant spacing $\Delta x = 0.35$ nm.[34] The solid atoms are uncharged and nonpolar, and the pairwise interaction energy due to van der Waals and hard–core interactions between the solid and liquid water ($\varepsilon_{SL} \simeq 0.83 k_B T$) is set to produce hydrophilic surfaces.

For the modeled system the solid atoms conforming the top and bottom walls are separated by an integer number j of lattice spacings and we thus define $z_w = (j/2)\Delta x - \Delta x/2$ as the approximate position of contact between water molecules and the solid wall, given that $\sigma \simeq \Delta x$. The height of the nanoscale water bridge in the MD simulations thus is $h = 2z_w$ (*cf.* Fig. 1b), considering that the top and bottom surfaces lie at the estimated position of contact between the water molecules and solid atoms where $|z| = z_w$. We performed MD simulations using sufficiently large numbers of water molecules ($N = 12\,000$–$36\,000$) so that for the modeled bridge heights $h = 4$–$19\ \Delta x$ and water volumes $V \simeq N/n_b = 0.37$–1.11 zL,[34] the characteristic bridge radius $R = \sqrt{V/\pi h} > 10\Delta x$ is always larger than ten molecule diameters. The local number density $n(z)$ and bridge radius $r(z)$ in MD simulations correspond to spatial averages over uniformly spaced slabs of thickness $\Delta x/2$, with additional time averaging over the final 2 ns of the simulation, which produced relative standard deviations smaller than 5% in all cases. The bridge radius is determined from the polar moment of area for the oxygen atoms, assuming a constant number density within each slab.[34]

Results and discussion

To assess the dual effect of hydration, we compare the local radius $r(z)$, slope $\dot{r}(z)$, and adhesion force $F(h)$ obtained from the MD simulations with: (YLA) The augmented Y–L equation with local pressure variation (eqn (1) and (2)) and the boundary conditions $\dot{r}(0) = 0$ and $\dot{r}(h/2) = \cot[\theta_Y(h)]$, given by eqn (3); and (YL) the conventional Y–L equation (eqn (1)) with a uniform liquid pressure and the boundary conditions $\dot{r}(0) = 0$, and $\dot{r}(h/2) = \cot[\theta_Y(h)]$, where θ_Y is either given by eqn (3) or the constant value $\theta_Y = 27.5^\circ$ observed in MD simulations for $h \gtrsim 20\Delta x$. The numerical solution of the Y–L equation (eqn (1)) is performed by a collocation method in MATLAB.

The number density profile

A knowledge of the local number density in the liquid phase is required to determine the local pressure (eqn (2)) and equilibrium contact angle (eqn (3)). Here, to model the effect of molecular layering and surface hydration we employ the approximate expression

$$n(z) = n_b + (n_1 - n_b) \times \left(e^{-\frac{d_+}{\Delta x}} \cos\frac{2\pi d_+}{\Delta x} + e^{-\frac{d_-}{\Delta x}} \cos\frac{2\pi d_-}{\Delta x} \right) \quad (5)$$

for $|z| \le h/2 - \delta$, where $d_\pm = h/2 - \delta \mp |z|$, and n_1 and δ are the number density and thickness, respectively, of the first hydration layer adjacent to the top/bottom wall located at $z = \pm z_w$ (see Fig. 1b). The sharp decay of the number density between the first hydration layer and the solid surface, where hard–core repulsion dominates, is defined by a heuristic expression $n(z) = n_1(1 + \tanh \kappa d)$ for $h/2 - \delta > |z| > h/2$, with $d = h/2 - \delta + (n_1/n_w)\Delta x - |z|$ and $\kappa = (\Delta x/20)^{-1}$, which enforces that $\int_0^{h/2} n(z)\mathrm{d}z = n_b \times (h/2)$ to satisfy mass conservation.

The heuristic expression for the number density in eqn (5) is analogous to those previously proposed[30,39] to model the disjoining pressure and oscillatory structural forces associated with surface hydration and molecular layering. While our MD simulations model both van der Waals, as well as structural and entropic forces, the expression in eqn (5) considers that hydration forces due to molecular layering are dominant. This assumption is justified for the modeled system for which relatively weak van der Waals interactions between the solid and liquid decay with $d_\pm^{-3}$ (here, $d_\pm$ is the distance from either wall).

The number density n_1 and thickness δ are here treated as adjustable model parameters to approximately fit the results from MD simulations. The values of n_1 and δ employed for analytical estimates *via* eqn (2)–(5) are reported in Table 1, and are consistent with values reported for water on hydrophilic surfaces.[17,29,40,41] For the studied conditions, for which $r(z) \gg \sigma$, the number density profiles and equilibrium contact angles obtained from MD simulations show no significant variation with respect to the bridge volume, while they are markedly influenced by the variation of the bridge height.[34]

Table 1 Model parameters: number density n_1 and thickness δ of the first hydration layer employed for analytical estimates for different bridge heights h (n_b = 0.0322 Å^{-3}, Δx = 0.35 nm). The height-dependent contact angle $\theta_Y(h)$ is given by eqn (3) using eqn (5) for the number density

$h/\Delta x$	n_1/n_b	$\delta/\Delta x$	θ_Y [deg]
4	1.83	0.715	52.7
6	1.86	0.725	47.3
9	1.88	0.8	37.6
14	1.91	0.84	32.8
19	1.92	0.87	27.5

The radius profile and contact angle

In Fig. 2 we compare the number density profile $n(z)$ modeled by eqn (5), and the local radius $r(z)$ and slope $\dot{r}(z)$ predicted by the YL and YLA models with their counterparts obtained from MD simulations for the case of three different bridge heights ($h/\Delta x$ = 4, 9, and 19) and the smallest simulated volume ($V \simeq 0.37$ zL). The MD simulations report two main effects associated to surface hydration: (a) strong spatial oscillations in the local number density that notably influence the local bridge radius and slope profiles near the walls, and (b) a significant increase of about $\sim 25^\circ$ in the equilibrium contact angle as the water bridge height decreases below 20 molecular diameters (*cf.* Fig. 2). These two effects are accounted for by the YLA model (eqn (1)–(5)) using the number density n_1 and thickness δ in Table 1. As reported previously,[42] the conventional YL model assuming a uniform number density and a fixed equilibrium contact angle given by the Young contact angle $\theta_Y = 27.5^\circ$ for large wall separations can account within a 10% error for the local radius obtained from MD simulations even for bridge heights as small as 10 water molecules (*cf.* Fig. 2b and c). However, we find that the YL model fails to describe the local slope $\dot{r}(z)$ and free surface curvature when the bridge height becomes comparable to 10 molecular layers (*cf.* Fig. 2c). When supplemented with the height-dependent equilibrium contact angle $\theta_Y(h)$ predicted by eqn (3) as a boundary condition, the classical Y–L equation assuming Δp = const. can describe both the local radius and slope reported by MD simulations (*cf.* Fig. 2c).

The capillary force

To fully evaluate the effects of surface hydration, we report in Fig. 3 the adhesion forces $F(h)$ computed from MD simulations and predicted *via* eqn (4) by the YL and YLA models, *i.e.*, the Y–L equation assuming uniform or spatially varying liquid pressure, when using the fixed contact angle $\theta_Y = 27.5^\circ$ for

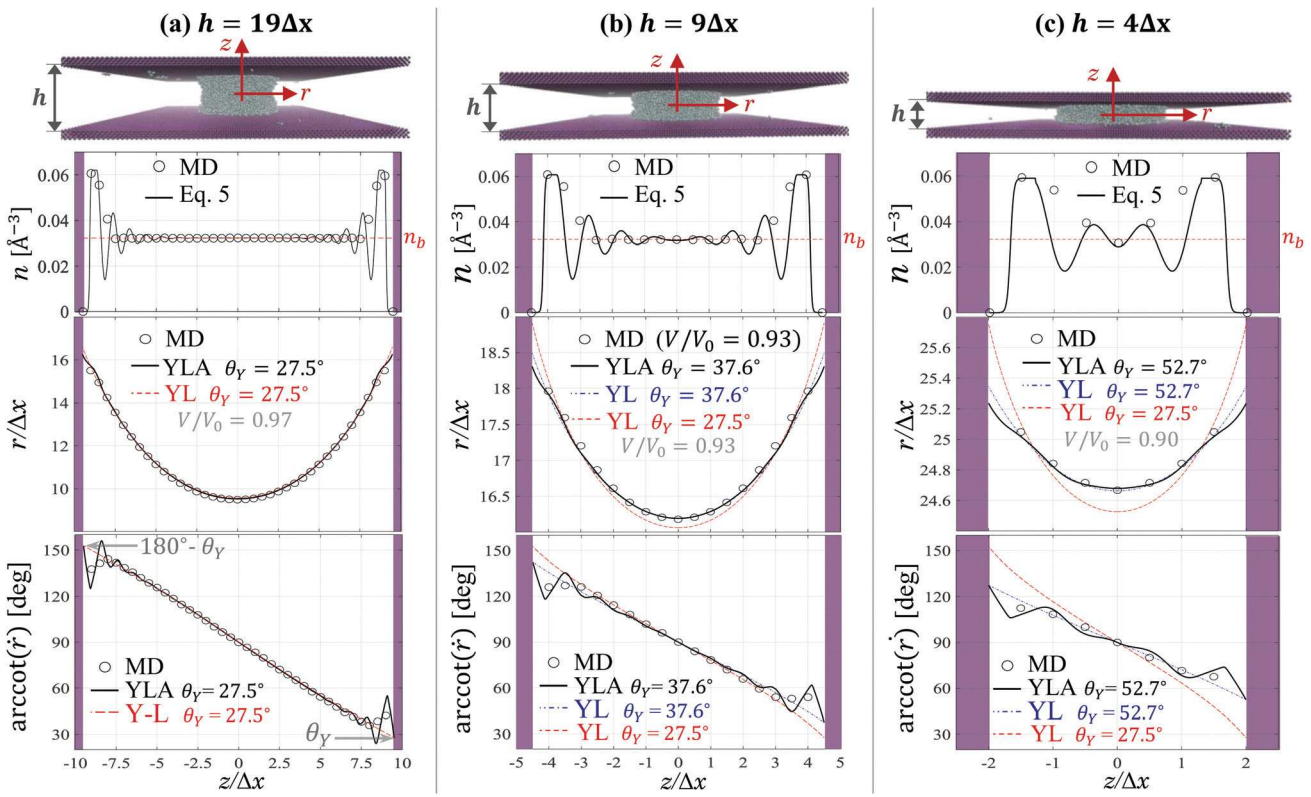

Fig. 2 Continuum descriptions and MD simulations of nanoscale water bridges: (a) $h = 19\Delta x \simeq 6.65$ nm ($V/V_0 = 0.97$), (b) $h = 9\Delta x \simeq 3.15$ nm ($V/V_0 = 0.93$), and (c) $h = 4\Delta x \simeq 1.4$ nm ($V/V_0 = 0.9$). The MD simulations are performed with N = 12 000 water molecules, which corresponds to the reference volume $V_0 = N/n_b = 0.37$ zL with $n_b = 0.0322$ Å^{-3}. Top panels are time snapshots from MD simulations, the graphs report the number density $n(z)$, bridge radius $r(z)$, and interface angle arccot($\dot{r}$). Analytical estimates from eqn (5) are obtained using the model parameters reported in Table 1. Continuum model predictions (see legend) correspond to numerical solutions of eqn (1) and (2): the augmented model (YLA) and the conventional Y–L equation (YL) using a variable and fixed Young contact angle.

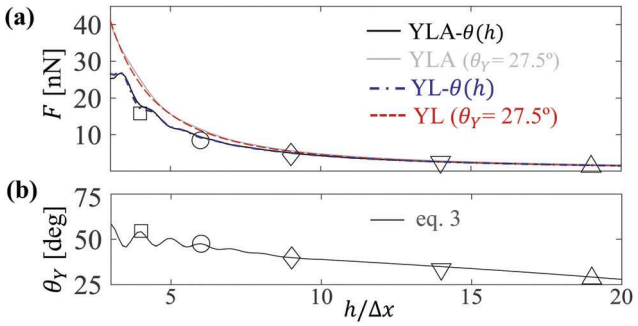

Fig. 3 Adhesion forces and surface hydration effects. (a) Adhesion forces reported by MD simulations and analytical estimates (see legend) *via* eqn (4) for: (YL) The Y–L equation with Δp = const. and the fixed contact angle $\theta_Y = 27.5^\circ$ or $\theta_Y(h)$ predicted by eqn (3); (YLA) The augmented Y–L equation (eqn (1) and (2)) with $\theta_Y = 27.5^\circ$ or $\theta_Y(h)$ predicted by eqn (3). (b) Height-dependent contact angle computed from MD simulations and predicted by eqn (3) using eqn (5) for the number density.

$h \gtrsim 20\Delta x$ and the height-dependent contact angle $\theta_Y(h)$ predicted by eqn (3). The analytical estimates *via* eqn (1)–(4) that are reported in Fig. 3a and b use a constant bridge volume $V = 0.37$ zL, and smooth functions $n_1(h)$ and $\delta(h)$ determined by piecewise cubic interpolation of the values reported in Table 1. Similar adhesion forces that show oscillations of small amplitude for $h \lesssim 10\Delta x$, are predicted by the YL and YLA models (Fig. 3a) when using the height-dependent contact angle $\theta_Y(h)$ reported in Fig. 3b. By comparing the forces predicted of the YL and YLA models (*cf.* Fig. 3a), we find that the spatial variation of the liquid pressure induced by the local density has a relatively small effect on the adhesion force. Furthermore, the YL and YLA models with the fixed contact angle observed for large heights predict a monotonic increase in the adhesion force with magnitudes that are up to 30% higher than reported by MD simulations (*cf.* Fig. 3a).

The adhesion forces predicted by the YL and YLA models show again that the most significant effect of the surface hydration phenomenon is the non-monotonic increase of the equilibrium contact angle (Fig. 3b) as the bridge height decreases. In the small height limit $h/V^{1/3} \to 0$, eqn (4) gives $F(h) = 2\gamma(V/h^2)\cos\theta_Y(h)$ and one can readily estimate the dimensionless adhesion force $\bar{F} = F(h)/F(h \to \infty) = \cos\theta_Y(h)/\cos\theta_Y(h \to \infty)$ and its relative decrease due to the effect of surface hydration on the contact angle. Contact angles $\theta_Y \simeq 20$–80° and $\bar{F} \simeq 0.3$–1 are predicted by eqn (3) when the number density and thickness of the first hydration layer vary within a physically meaningful range (*i.e.*, $n_1 = 1.7$–$2n_b$ and $\delta = 0.7$–$1\Delta x$) for water confined by hydrophilic surfaces.[29,40,41] The relative decrease of the adhesion force $\bar{F} < 1$ is more pronounced as the surface hydrophilicity decreases.

Conclusions

In conclusion, we have proposed an alternative sharp-interface continuum description for nanoscopically confined molecular liquids that is based on the Y–L equation by considering spatial variations of the number density and configuration-dependent liquid–solid surface energy due to surface hydration. We verified the model assumptions by comparing with MD simulation results for nanoscale water bridges with contact radii much larger than the molecular diameter. The proposed augmented description requires a knowledge of the local number density, which was here approximated by a simple heuristic expression considering the molecular layering of water molecules. The modeled surface hydration phenomenon produces (i) spatial variations of the local pressure and the curvature of a nanoscale capillary bridge and, more significantly, (ii) an equilibrium contact angle that varies with the distance between the confining surfaces. This dual effect of surface hydration is reported by MD simulations of water bridges with nanoscale heights and a sufficiently large volumes so that the bridge radius $r(z) > 10\sigma$ is larger than 10 molecular diameters. The dependence of the equilibrium contact angle with the bridge height is confirmed by both the changes in the radius slope $\dot{r}(z)$ and the adhesion forces reported by MD simulations when the height is smaller than 20 water molecules (*i.e.*, $h \lesssim 7$ nm) for the case of water bridges between neutrally charged and hydrophilic surfaces. By considering the variation of the equilibrium contact angle predicted by the proposed analytical expressions, the conventional Y–L equation assuming a perfectly homogeneous liquid phase at constant pressure was able to account for MD simulation results of capillary bridges with heights smaller than 10 water molecules and a sufficiently large volume so that the local bridge radius is larger than 10 molecular diameters. Our analysis showed that adhesion forces produced by nanoscale capillary bridges can be significantly overestimated by not considering the reported height-dependent and non-monotonic increase in the equilibrium contact angle as two surfaces approach contact.

The proposed augmented model can be readily employed with more accurate expressions for the local number density in the liquid that can be obtained by different theoretical or experimental methods. Accurate expressions for the local number density can thus model the combined effects of DLVO interactions and surface forces on the local pressure and the variation of the equilibrium contact angle for more complex systems than the case of water on neutrally charged hydrophilic surfaces studied in this work. The critical length below which the proposed augmented description considering the liquid structure near the confining surface is necessary can be generally much larger than a few molecular diameters. This critical length corresponds to the length over which the local liquid structure and number density present substantial spatial variations, and it is thus prescribed by the characteristic length of action of the dominant molecular and surface forces (*i.e.*, DLVO and non-DLVO interaction) between the liquid and confining solid. It is therefore worth noting that both the chemical physics and geometry of the system will determine the scales for which it is useful to employ the augmented description proposed in this work.

Conflicts of interest

There are no conflicts to declare.

Acknowledgements

This work was supported by the NSF under the collaborative award DMS-1614892 (CEC), DMS-1614863 (YNY), and DMS-1614907 (HAS). CEC acknowledges support by the NSF under award CBET-2016204. YNY acknowledges support by the NSF under award DMS-1412789 and The Flatiron Institute of The Simons Foundation.

Notes and references

1 M. Abi Ghanem, A. Khanolkar, S. P. Wallen, M. Helwig, M. Hiraiwa, A. A. Maznev, N. Vogel and N. Boechler, *Nanoscale*, 2019, **11**, 5655–5665.
2 K. Liu, I. Berbezier, L. Favre, A. Ronda, M. Abbarchi, P. Donnadieu, P. W. Voorhees and J.-N. Aqua, *Nanoscale*, 2019, **11**, 7798–7804.
3 S. Park, H. Hwang, M. Kim, J. H. Moon and S.-H. Kim, *Nanoscale*, 2020, **12**, 18576–18594.
4 J. Yin, Y. Huang, S. Hameed, R. Zhou, L. Xie and Y. Ying, *Nanoscale*, 2020, **12**, 17571–17589.
5 K. Park and H. Kim, *Nanoscale*, 2021, **13**, 14656–14665.
6 H. E. Jeong, R. Kwak, A. Khademhosseini and K. Y. Suh, *Nanoscale*, 2009, **1**, 331–338.
7 D. Ho, J. Zou, B. Zdyrko, K. S. Iyer and I. Luzinov, *Nanoscale*, 2015, **7**, 401–414.
8 K. Zhang, J. Li, Y. Fang, B. Luo, Y. Zhang, Y. Li, J. Zhou and B. Hu, *Nanoscale*, 2018, **10**, 12981–12990.
9 Y. Liu, Y. Zhang, S. Ortega, M. Ibáñez, K. H. Lim, A. Grau-Carbonell, S. Mart-Sánchez, K. M. Ng, J. Arbiol and M. V. Kovalenko, *et al.*, *Nano Lett.*, 2018, **18**, 2557–2563.
10 S. Roh, D. P. Parekh, B. Bharti, S. D. Stoyanov and O. D. Velev, *Adv. Mater.*, 2017, **29**, 1701554.
11 H. Ding, S. Barg and B. Derby, *Nanoscale*, 2020, **12**, 11440–11447.
12 C. Yan, P. Jiang, X. Jia and X. Wang, *Nanoscale*, 2020, **12**, 2924–2938.
13 S. Kwon, C. Stambaugh, B. Kim, S. An and W. Jhe, *Nanoscale*, 2014, **6**, 5474–5478.
14 T. Jiang and Y. Zhu, *Nanoscale*, 2015, **7**, 10760–10766.
15 M. Dehnert and R. Magerle, *Nanoscale*, 2018, **10**, 5695–5707.
16 E. Liamas, S. D. Connell, S. N. Ramakrishna and A. Sarkar, *Nanoscale*, 2020, **12**, 2292–2308.
17 M. R. Uhlig and R. Garcia, *Nano Lett.*, 2021, **21**, 5593–5598.
18 P. A. Kralchevsky and N. D. Denkov, *Curr. Opin. Colloid Interface Sci.*, 2001, **6**, 383–401.
19 H.-J. Butt and M. Kappl, *Adv. Colloid Interface Sci.*, 2009, **146**, 48–60.
20 C. Huang and Z. Guo, *Nanoscale*, 2018, **10**, 19659–19672.
21 C. E. Colosqui, *Encycl. Interfacial Chem.*, 2018, 654–667, DOI: **10.1016/B978-0-12-409547-2.13230-5**, **https://www.sciencedirect.com/science/article/pii/B9780124095472132305**.
22 P.-G. De Gennes, *Rev. Mod. Phys.*, 1985, **57**, 827.
23 G. Hirasaki, *SPE Form. Eval.*, 1991, **6**, 217–226.
24 V. Starov and M. Velarde, *J. Condens. Matter Phys.*, 2009, **21**, 464121.
25 S. Kelly, C. Torres-Verdn and M. T. Balhoff, *Nanoscale*, 2016, **8**, 2751–2767.
26 A. A. Pahlavan, L. Cueto-Felgueroso, A. E. Hosoi, G. H. McKinley and R. Juanes, *J. Fluid Mech.*, 2018, **845**, 642–681.
27 J. Mo, J. Sha, D. Li, Z. Li and Y. Chen, *Nanoscale*, 2019, **11**, 8408–8415.
28 J. N. Israelachvili and R. M. Pashley, *Nature*, 1983, **306**, 249–250.
29 S.-H. Park and G. Sposito, *Phys. Rev. Lett.*, 2002, **89**, 085501.
30 J. N. Israelachvili, *Intermolecular and surface forces*, Academic Press, 2011.
31 R. M. Pashley and J. N. Israelachvili, *J. Colloid Interface Sci.*, 1984, **101**, 511–523.
32 J. N. Israelachvili and P. M. McGuiggan, *Science*, 1988, **241**, 795–800.
33 S. Plimpton, P. Crozier and A. Thompson, *Sandia Natl. Lab.*, 2007, **18**, 43.
34 See ESI,† for details on the molecular dynamics simulations performed in this work.
35 H. W. Horn, W. C. Swope, J. W. Pitera, J. D. Madura, T. J. Dick, G. L. Hura and T. Head-Gordon, *J. Chem. Phys.*, 2004, **120**, 9665–9678.
36 H. W. Horn, W. C. Swope and J. W. Pitera, *J. Chem. Phys.*, 2005, **123**, 194504.
37 C. Vega, J. Abascal and I. Nezbeda, *J. Chem. Phys.*, 2006, **125**, 034503.
38 C. Vega and E. De Miguel, *J. Chem. Phys.*, 2007, **126**, 154707.
39 P. A. Kralchevsky and N. D. Denkov, *Chem. Phys. Lett.*, 1995, **240**, 385–392.
40 L. Cheng, P. Fenter, K. L. Nagy, M. L. Schlegel and N. C. Sturchio, *Phys. Rev. Lett.*, 2001, **87**, 156103.
41 P. Fenter and S. S. Lee, *MRS Bull.*, 2014, **39**, 1056.
42 S. Cheng and M. O. Robbins, *Langmuir*, 2016, **32**, 7788–7795.